

A&A manuscript no.
 (will be inserted by hand later)

Your thesaurus codes are:
03(02.01.2; 11.01.2; 11.14.1; 11.19.1; 11.17.3)

**ASTRONOMY
 AND
 ASTROPHYSICS**

X-ray variability in a complete sample of Soft X-ray selected AGN *

D. Grupe^{1,**}, H.-C. Thomas², and K. Beuermann^{1,3},

¹ MPI für extraterrestrische Physik, Postfach 1312, 85741 Garching, FRG

² MPI für Astrophysik, Karl-Schwarzschild-Str. 1, 85741 Garching, FRG

³ Universitäts-Sternwarte, Geismarlandstr. 11, 37083 Göttingen, FRG

Received 11 August 2000; Accepted 04 December 2000

Abstract. We present ROSAT All-Sky Survey and ROSAT pointed observations (PSPC and HRI) of a complete sample of 113 bright soft X-ray AGN selected from the ROSAT Bright Source Catalog. We compare these observations in order to search for extreme cases of flux and spectral X-ray variability - X-ray transient AGN. Three definite transients and one transient candidate are found. The other sources show amplitude variations typically by factors of 2-3 on timescales of years. We found that the variability strength on timescales of days is a function of the steepness of the X-ray spectrum: steeper X-ray objects show stronger variability than flat X-ray spectrum sources. We also present new HRI measurements of our extreme X-ray transients IC 3599 and WPVS007. We discuss possible models to explain the X-ray transience and the variabilities observed in the non-transient sources.

Key words: accretion, accretion disks – galaxies: active – galaxies: nuclei of – galaxies: Seyfert – quasars: general

1. Introduction

The optical-UV-soft X-ray bump has turned out to be a common property of most Narrow-Line Seyfert 1 (NLS1) type Active Galactic Nuclei (AGN). With ROSAT's (Trümper 1983) Position Sensitive Proportional Counter (PSPC, Pfeffermann et al. 1986) with its spectral sensitivity to energies below 0.5 keV, numerous AGN have been found that show a soft X-ray excess, commonly believed to be the high energy part of the "Big Blue/UV Bump". This bump emission is thought to be produced by an accretion disk that surrounds the central black hole. The soft X-ray

Send offprint requests to:

D. Grupe (dgrupe@xray.mpe.mpg.de)

* Based in part on observations at the European Southern Observatory La Silla (Chile) with the 2.2m telescope of the Max-Planck-Society during MPG and ESO time and the ESO 1.52m telescope.

** Guest Observer, McDonald Observatory, University of Texas at Austin

emission is explained by Compton scattering of thermal UV disk photons by a hot electron layer above the disk. The UV photon spectrum is shifted further into the soft X-ray range as the engine accretes closer to its Eddington accretion rate (e.g. Ross et al. 1992). Before ROSAT, a study of soft X-ray selected AGN had to rely on serendipitous observations, notably with the EINSTEIN Image Proportional Counter (Córdova et al. (1992), Puchnarewicz et al. (1992))

The ROSAT All-Sky Survey (RASS, Voges et al. 1999) and later re-observations of many sources made it possible to study the long-term behaviour of AGN in X-rays. AGN can vary in three ways, either by changes in the flux (or count rate), solely by spectral changes, or a combination of both. Most common are variations in X-ray flux by factors of 2-3 on timescales of days and years (e.g. Lawrence et al. 1977, Green et al. 1993, Boller et al. 1996). However, factors of more than ten have been reported for several sources (e.g. IRAS 13224–3809, Boller et al. 1997 or PHL 1092, Brandt et al. 1999). AGN can also change the shape of their X-ray spectra. The most extreme example of such a spectral change has been reported on the Narrow-line Seyfert 1 galaxy (NLS1) RX J0134.2–4258 (Grupe et al. 2000a, Komossa & Meierschweinchen 2000). It has been shown that the timescales of the variabilities found in AGN scale with luminosity (Barr & Mushotzky 1986, Lawrence & Papadakis 1993, Green et al. 1993). Leighly (1999a,b) has presented a comprehensive variability study on a sample of 25 AGN observed by ASCA and found a) that the variability strength is a function of the luminosity and b) that NLS1 are more variable than Broad-Line Seyfert 1s. Boller et al. (1996) found in their NLS1 study based on ROSAT data that the timescale of the variability is a function of the luminosity. Variability in X-rays can be due either to changes in the absorption column or intrinsic variability of the X-ray source. Absorption by both neutral and ionized gas has been proposed to explain the X-ray variability observed (see Abrassart & Czerny 2000 and Komossa & Meierschweinchen 2000). Intrinsic variability can be caused by e.g. changes in the accretion rate or relativistic beaming effects (e.g. Boller et al. 1997).

With the RASS a new AGN phenomenon has been established: X-ray transience. X-ray transience is the most extreme form of variability in AGN. On timescales of years, the count rates decreased by factors of more than 100 or the sources even vanished in X-rays. The first example of an X-ray transient AGN was given by Piro et al. (1988) who reported a change in the soft X-ray luminosity of the Seyfert 1 galaxy E1615+061 by two orders of magnitude on timescales of years. Transient sources are thought to accrete at high rates, close to the Eddington limit, and therefore have very soft X-ray spectra. The RASS with its sensitivity to energies down to 0.1 keV has a high potential to find transient sources. Transience in AGN can be caused by changes of accretion disk properties (e.g. the temperature, see WPVS007, Grupe et al. 1995b), a dramatic increase of the accretion rate (e.g. in an outburst as seen in IC 3599, Brandt et al. 1995, Grupe et al. 1995a), or alternatively, changes in the absorption column in the line of sight.

Thomas et al. (1998) have presented a completely identified sample of all 397 bright soft X-ray selected, high galactic latitude RASS sources (mean PSPC count rate $\geq 0.5 \text{ cts s}^{-1}$, hardness ratio 1 (HR1) $< 0.00^1$, and $|b| > 20^\circ$, based on RASS II). Of these sources, 113 are AGN, which is the sample we present here. Our sample is complete for all AGN following the criteria above. BL Lac objects were excluded because of their different X-ray emission mechanism.

The task of this new paper is to compare the RASS results with measurements of ROSAT pointed observations in order to find new X-ray transient AGN. In Sect. 2 we describe the observations and data reduction. Sect. 3 shows the results obtained for the whole sample and lists individual X-ray transient AGN, and in Sect. 4 we discuss the results. Throughout the paper, luminosities are calculated assuming a Hubble constant of $H_0 = 75 \text{ km s}^{-1} \text{Mpc}^{-1}$ and a deceleration parameter of $q_0 = 0$. Spectral slopes, α , are defined by $F \propto \nu^{-\alpha}$.

2. Observations and data reduction

All objects have been observed (by definition) during the RASS. The data from RASS II² were extracted from the event files as described in Grupe et al. (1998a). Pointed PSPC and High Resolution Imager (HRI) observations were derived from the ROSAT public data archive at MPE Garching (<ftp://xray.mpe.mpg.de>). The source PSPC count rates were determined using a weighted exposure map in four energy channel ranges, 8-41, 42-51, 52-90, and 91-

¹ The hardness ratio is defined as $\text{HR1} = (\text{hard-soft})/(\text{hard+soft})$ with soft PSPC channels = 11-41 and hard = 52-201.

² The difference between RASS I and RASS II is in the detection likelihood for acceptance of a source; Voges et al. 1999. Meanwhile the RASS III has been released.)

201³. Power-law spectral models were applied to the RASS as well as to the pointed PSPC data. We limit the spectral analysis to single power-law fits only because of the limited signal-to-noise ratios of the RASS observations. The absorption parameter for cold absorption N_H was either fixed to the Galactic value given by Dickey & Lockman (1990), or left as a free parameter (see Table 4).

In cases where more than one pointed PSPC (or HRI) observation was available in the archive, we usually took the longest one in order to get better signal-to-noise ratio. HRI count rates were converted into effective PSPC count rates using the W3PIMMS program of NASA's Goddard Space Flight Center (version 2.7, 1999, <http://heasarc.gsfc.nasa.gov/Tools/w3pimms.html>) based on the power-law fits to the RASS data with the absorption parameter N_H fixed to the galactic value, and assuming no spectral changes between the RASS and the HRI observations. For all X-ray reduction and analysis tasks we used the EXSAS data analysis package of the MPE Garching (5th edition, Zimmermann et al. 1998).

3. Results

Table 1 lists the optical coordinates derived from the US Naval Observatory scans (USNO A2.0) and summarizes the count rates and hardness ratios of the RASS, pointed PSPC, and HRI observations. The X-ray positions of the objects are given in Thomas et al. (1998). The RASS count rates and HR1 given in Table 1 differ slightly from the values in the ROSAT Bright Source Catalogue (BSC, Voges et al. 1999), because while the definition of the sample is based on the BSC our analysis of the RASS event files were used for all analysis throughout the paper. In two cases (RX J1624.9+7554 and RX J2312.5-3404) the count rates are below the limit of 0.5 cts s^{-1} and in one case, IIZW136, the HR1 > 0.00 . All observations used for this publication, with their observing dates, exposure times and the ROSAT Observation Request number (ROR) of the pointed observations, are listed in Table 2.

3.1. Flux variability

Fig. 1 compares the RASS vs. PSPC and HRI pointed observation count rates. In general, if PSPC and HRI observations were available for one source, preference was given to the PSPC observation, because RASS and PSPC pointings were performed by the same type of detector and allow, therefore, a direct comparison without any assumptions about the spectral shape that is necessary for converting the HRI observations. The plot displays that the distribution of the converted HRI count rates does not differ significantly from the PSPC data. It shows that the method of conversion is basically correct.

³ One energy channel transfers to 10 eV

Table 1. Optical positions of the AGN taken from the USNO, RASS and pointed observation count rates and hardness ratios. For the HRI observations expected HRI count rates derived from the RASS observations and expected PSPC count rates are listed.

No.	α_{2000}	δ_{2000}	Name	z	RASS		PSPC pointed		HRI pointed	
					CR cts s ⁻¹	HR1	CR cts s ⁻¹	HR1	expected HRI CR	CR cts s ⁻¹
h m s	°' "									converted CR
1	00 06 19.5	+20 12 11	Mkn 335	0.026	2.33±0.10	-0.07±0.04	2.60±0.01	-0.04±0.02	0.660	0.426±0.007
2	00 25 00.2	-45 29 34	ESO 242-G8	0.059	0.79±0.08	-0.48±0.07	0.47±0.01	-0.43±0.09	0.183	0.060±0.006
3	00 39 15.8	-51 17 02	WPVS 007	0.029	0.96±0.07	-0.97±0.02	0.002±0.001	¹	0.197	0.001
4	00 57 20.2	-22 22 57	RX J0057.2-2223	0.062	2.72±0.10	-0.58±0.03	3.28±0.03	-0.59±0.05	—	—
5	00 58 37.4	-36 06 05	QSO 0056-36	0.165	0.75±0.06	-0.31±0.06	—	—	0.178	0.162±0.008
6	01 00 27.1	-51 13 54	RX J0100.4-5113	0.062	1.06±0.08	-0.24±0.07	—	—	0.272	0.127±0.005
7	01 05 38.8	-14 16 14	RX J0105.6-1416	0.070	1.56±0.07	-0.17±0.04	—	—	—	—
8	01 17 30.6	-38 26 30	RX J0117.5-3826	0.225	0.98±0.07	-0.52±0.04	—	—	—	—
9	01 19 35.7	-28 21 32	MS 0117-28	0.349	0.60±0.06	-0.72±0.05	0.48±0.01	-0.79±0.02	—	—
10	01 28 06.7	-18 48 31	RX J0128.1-1848	0.046	0.76±0.06	-0.28±0.06	—	—	—	—
11	01 29 10.7	-21 41 57	IRAS F01267-217	0.093	0.83±0.07	-0.45±0.06	—	—	0.192	0.482±0.011
12	01 48 22.3	-27 58 26	RX J0148.3-2758	0.121	2.35±0.09	-0.62±0.03	1.63±0.02	-0.51±0.05	—	—
13	01 52 27.1	-23 19 54	RX J0152.4-2319	0.113	1.08±0.06	-0.52±0.04	—	—	0.223	0.241±0.007
14	02 30 05.5	-08 59 53	Mkn 1044	0.017	2.23±0.10	-0.06±0.04	2.10±0.03	-0.02±0.05	—	—
15	02 34 37.8	-08 47 16	Mkn 1048	0.042	1.24±0.08	-0.05±0.06	1.30±0.02	+0.04±0.05	0.355	0.106±0.008
16	03 11 18.8	-20 46 19	RX J0311.3-2046	0.070	0.91±0.08	-0.08±0.07	—	—	—	—
17	03 19 48.7	-26 27 12	RX J0319.8-2627	0.079	0.52±0.07	-0.52±0.09	0.78±0.01	-0.35±0.06	—	—
18	03 23 15.8	-49 31 11	RX J0323.2-4931	0.071	1.45±0.06	-0.50±0.03	0.50±0.01	-0.46±0.08	0.304	0.094±0.007
19	03 25 02.2	-41 54 18	ESO 301-G13	0.059	0.96±0.06	-0.48±0.04	—	—	0.219	0.371±0.012
20	03 33 40.2	-37 06 55	VCV0331-37	0.064	0.68±0.08	-0.40±0.09	—	—	0.159	0.142±0.007
21	03 49 07.7	-47 11 04	RX J0349.1-4711	0.299	0.53±0.06	-0.70±0.05	—	—	0.095	0.044±0.005
22	03 51 41.7	-40 28 00	Fairall 1116	0.059	1.86±0.14	-0.37±0.06	—	—	0.474	0.205±0.009
23	04 05 01.7	-37 11 15	CTS 44	0.055	3.29±0.11	-0.37±0.02	—	—	—	—
24	04 12 41.5	-47 12 46	RX J0412.7-4712	0.132	0.77±0.10	-0.52±0.09	—	—	0.169	0.261±0.008
25	04 26 00.7	-57 12 02	1H 0419+577	0.104	3.63±0.10	-0.54±0.02	6.00±0.04	-0.47±0.03	0.795	0.510±0.011
26	04 30 40.0	-53 36 56	Fairall 303	0.040	1.18±0.09	-0.50±0.06	0.99±0.02	-0.39±0.09	—	—
27	04 37 28.2	-47 11 30	RX J0437.4-4711	0.052	1.13±0.06	-0.60±0.03	1.35±0.02	-0.51±0.05	0.230	0.461±0.005
28	04 39 38.7	-53 11 31	RX J0439.6-5311	0.243	0.83±0.12	-0.81±0.06	1.44±0.02	-0.79±0.02	—	—
29	04 41 22.5	-27 08 20	H 0439-272	0.084	0.62±0.10	-0.09±0.12	0.77±0.01	+0.09±0.07	—	—
30	06 15 49.6	-58 26 06	1 ES 0614-584	0.057	0.59±0.04	-0.18±0.03	—	—	—	—
31	08 59 02.9	+48 46 09	RX J0859.0+4846	0.083	0.70±0.06	-0.18±0.07	—	—	—	—
32	09 02 33.6	-07 00 04	RX J0902.5-0700	0.089	0.62±0.06	-0.22±0.07	—	—	—	—
33	09 25 13.0	+52 17 12	Mkn 110	0.035	1.65±0.08	-0.21±0.04	6.30±0.03	-0.28±0.02	0.420	1.519±0.008
34	09 56 52.4	+41 15 22	PG 0953+41	0.234	0.99±0.07	-0.56±0.04	0.76±0.01	-0.49±0.07	—	—
35	10 05 41.9	+43 32 41	RX J1005.7+4332	0.178	0.73±0.05	-0.64±0.04	—	—	0.143	0.052±0.004
36	10 07 10.2	+22 03 02	RX J1007+2203	0.083	0.62±0.06	-0.09±0.06	—	—	—	—
37	10 13 03.2	+35 51 24	CBS 126	0.079	1.43±0.07	-0.45±0.03	—	—	0.316	0.055±0.005
38	10 19 00.5	+37 52 41	HS 1019+37	0.135	0.81±0.06	-0.08±0.05	0.37±0.01	+0.02±0.03	—	—
39	10 19 12.6	+63 58 03	Mkn 141	0.042	0.50±0.06	-0.45±0.06	—	—	0.108	0.032±0.004
40	10 25 31.3	+51 40 35	Mkn 142	0.045	1.73±0.07	-0.62±0.03	1.44±0.02	-0.56±0.05	—	0.149

No.	α_{2000} h m s	δ_{2000} $^{\circ} \text{ } '$ "	Name	z	RASS		PSPC pointed		HRI pointed		
					CR cts s^{-1}	HR1	CR cts s^{-1}	HR1	expected	CR cts s^{-1}	converted
41	10 34 38.6	+39 38 28	RX J1034.6+3938	0.044	2.62±0.10	-0.74±0.02	3.53±0.03	-0.71±0.04	—	—	—
42	11 17 10.1	+65 22 07	RX J1117.1+6522	0.147	0.58±0.05	-0.72±0.04	—	—	0.108	0.060±0.007	0.325
43	11 18 30.4	+40 25 55	PG 1115+407	0.154	0.56±0.06	-0.46±0.06	0.32±0.01	-0.51±0.10	0.121	0.068±0.005	0.315
44	11 19 08.7	+21 19 18	Ton 1388	0.177	1.00±0.08	-0.53±0.05	1.05±0.01	-0.46±0.03	0.213	0.339±0.014	1.594
45	11 31 04.8	+68 51 53	EXO 1128+69	0.045	1.59±0.06	-0.45±0.03	—	—	—	—	—
46	11 31 09.5	+31 14 06	B2 1128+31	0.289	0.56±0.06	-0.11±0.08	—	—	—	—	—
47	11 38 49.6	+57 42 44	SBS 1136+579	0.116	0.60±0.06	-0.47±0.06	0.16±0.01	-0.63±0.22	—	—	—
48	11 39 13.9	+33 55 51	Z 1136+3412	0.033	0.85±0.07	-0.33±0.06	0.64±0.02	-0.42±0.15	—	—	—
49	11 41 16.2	+21 56 21	Was 26	0.063	1.60±0.07	-0.13±0.04	0.98±0.02	-0.11±0.06	—	—	—
50	11 44 29.9	+36 53 09	CASG 855	0.040	1.29±0.08	-0.18±0.05	—	—	—	—	—
51	12 01 14.4	-03 40 41	Mkn 1310	0.019	0.89±0.06	-0.07±0.06	0.26±0.01	-0.06±0.16	—	—	—
52	12 03 09.5	+44 31 50	NGC 4051	0.002	3.62±0.11	-0.47±0.02	1.68±0.01	-0.41±0.02	0.804	0.489±0.014	2.209
53	12 04 42.1	+27 54 12	GQ Com	0.165	0.59±0.05	-0.13±0.06	0.47±0.01	-0.11±0.04	0.158	0.164±0.008	0.613
54	12 09 45.2	+32 17 02	RX J1209.8+3217	0.145	0.59±0.11	-0.63±0.08	0.28±0.01	-0.58±0.18	—	—	—
55	12 14 17.7	+14 03 13	PG1211+14	0.082	1.71±0.08	-0.35±0.03	1.05±0.02	-0.20±0.06	—	—	—
56	12 18 26.6	+29 48 46	Mkn 766	0.013	5.35±0.13	-0.03±0.02	3.53±0.02	-0.09±0.03	1.468	0.384±0.002	1.399
57	12 29 06.7	+02 03 09	3C 273	0.158	7.54±0.16	-0.15±0.02	6.29±0.03	+0.10±0.02	1.988	3.082±0.039	11.69
58	12 31 36.6	+70 44 14	RX J1231.6+7044	0.208	1.08±0.05	-0.20±0.04	—	—	0.273	0.162±0.007	0.642
59	12 32 03.6	+20 09 30	Mkn 771	0.064	0.61±0.05	-0.39±0.06	1.32±0.02	-0.26±0.05	—	—	—
60	12 33 41.7	+31 01 03	CBS 150	0.290	0.51±0.05	-0.53±0.05	0.33±0.01	-0.53±0.15	—	—	—
61	12 36 51.2	+45 39 05	MCG+08-23-067	0.030	0.58±0.05	-0.29±0.06	—	—	—	—	—
62	12 37 41.2	+26 42 28	IC 3599	0.021	4.90±0.11	-0.64±0.02	0.07±0.01	-0.83±0.05	1.247	0.005±0.001	0.025
63	12 39 39.4	-05 20 39	NGC 4593	0.009	3.32±0.18	-0.16±0.05	1.44±0.04	+0.10±0.10	0.897	1.041±0.024	3.850
64	12 42 10.6	+33 17 03	IRAS F12397+3333	0.044	0.84±0.06	-0.33±0.05	0.78±0.01	-0.27±0.05	—	—	—
65	12 46 35.2	+02 22 09	PG 1244+026	0.049	1.28±0.10	-0.50±0.06	1.15±0.02	-0.44±0.05	—	—	—
66	13 04 17.0	+02 05 37	RX J1304.2+0205	0.229	0.79±0.07	-0.64±0.05	—	—	—	—	—
67	13 09 47.0	+08 19 48	PG 1307+085	0.155	0.60±0.06	-0.24±0.06	0.56±0.01	-0.24±0.06	0.153	0.100±0.006	0.395
68	13 14 22.7	+34 29 39	RX J1314.3+3429	0.075	0.68±0.06	-0.62±0.04	0.74±0.03	-0.70±0.20	0.128	0.117±0.005	0.620
69	13 19 57.1	+52 35 33	RX J1319.9+5235	0.092	0.68±0.05	-0.53±0.05	—	—	—	—	—
70	13 23 49.5	+65 41 48	PG 1322+659	0.168	0.71±0.05	-0.48±0.04	0.54±0.01	-0.39±0.07	—	—	—
71	13 37 18.7	+24 23 03	IRAS 1334+24	0.108	2.50±0.09	-0.66±0.03	1.04±0.02	-0.61±0.09	0.485	0.319±0.008	1.644
72	13 43 56.7	+25 38 48	Ton 730	0.087	0.55±0.05	-0.60±0.05	—	—	—	—	—
73	13 55 16.6	+56 12 45	RX J1355.2+5612	0.122	0.71±0.06	-0.63±0.04	—	—	0.137	0.122±0.008	0.634
74	14 05 16.2	+25 55 34	PG 1402+25	0.164	0.66±0.05	-0.55±0.05	0.99±0.02	-0.56±0.10	0.140	0.337±0.009	1.590
75	14 13 36.7	+70 29 50	RX J1413.6+7029	0.107	0.76±0.07	-0.16±0.06	—	—	0.199	0.105±0.006	0.401
76	14 17 59.5	+25 08 12	NGC 5548	0.017	4.76±0.11	-0.14±0.02	7.95±0.03	-0.19±0.02	1.270	0.763±0.019	2.857
77	14 24 03.8	-00 26 58	QSO 1421-0013	0.151	0.58±0.06	-0.06±0.07	—	—	—	—	—
78	14 27 25.0	+19 49 53	Mkn 813	0.111	0.79±0.06	-0.14±0.05	—	—	—	—	—
79	14 31 04.1	+28 17 14	Mkn 684	0.046	0.53±0.06	-0.24±0.07	—	—	0.131	0.247±0.010	1.002
80	14 42 07.5	+35 26 23	Mkn 478	0.077	5.31±0.11	-0.73±0.01	3.17±0.05	-0.75±0.09	0.958	0.119±0.004	0.660

No.	α_{2000}	δ_{2000}	Name	z	RASS		PSPC pointed		HRI pointed		
					CR cts s ⁻¹	HR1	CR cts s ⁻¹	HR1	expected HRI CR	CR cts s ⁻¹	converted CR
h m s	° ' "										
81	14 51 08.8	+27 09 27	PG 1448+273	0.065	0.78±0.06	-0.03±0.05	—	—	—	—	—
82	15 04 01.2	+10 26 16	Mkn 841	0.036	0.77±0.08	-0.18±0.06	2.20±0.01	-0.07±0.02	0.205	0.888±0.019	3.303
83	15 29 07.5	+56 16 07	HS 1529+56	0.100	0.79±0.05	-0.46±0.03	—	—	—	—	—
84	15 59 09.7	+35 01 48	Mkn 493	0.032	0.55±0.06	-0.24±0.07	0.40±0.01	-0.23±0.07	—	—	—
85	16 13 57.2	+65 43 11	Mkn 876	0.129	0.84±0.05	-0.08±0.03	0.98±0.01	-0.04±0.05	—	—	—
86	16 18 09.4	+36 19 58	RX J1618.1+3619	0.034	0.87±0.05	-0.44±0.03	—	—	0.193	0.113±0.005	0.509
87	16 19 51.3	+40 58 48	KUG 1618+40	0.038	0.57±0.06	-0.56±0.04	—	—	—	—	—
88	16 24 56.6	+75 54 56	RX J1624.9+7554	0.065	0.44±0.04	-0.22±0.04	³	³	—	—	—
89	16 27 56.1	+55 22 32	PG 1626+554	0.133	0.61±0.05	-0.37±0.04	1.05±0.02	-0.49±0.09	—	—	—
90	16 29 01.3	+40 08 00	EXO 1627+4014	0.272	0.84±0.05	-0.80±0.02	0.99±0.01	-0.77±0.09	—	—	—
91	17 02 31.1	+32 47 20	HS 1702+32	0.164	0.58±0.05	-0.48±0.04	0.81±0.01	-0.62±0.07	—	—	—
92	21 32 27.9	+10 08 20	II Zw 136	0.065	1.30±0.07	+0.01±0.04	1.16±0.02	+0.08±0.04	0.393	0.265±0.011	0.874
93	21 46 36.0	-30 51 41	RX J2146.6-3051	0.075	0.77±0.06	-0.14±0.06	—	—	—	—	—
94	22 07 45.0	-32 35 01	A 09.25	0.063	0.98±0.07	-0.25±0.06	—	—	—	—	—
95	22 09 07.6	-27 48 36	NGC 7214	0.023	0.78±0.08	-0.25±0.07	2.69±0.01	-0.40±0.02	0.198	0.133±0.02	0.525
96	22 16 53.2	-44 51 57	RX J2216.8-4451	0.136	1.39±0.08	-0.66±0.03	—	—	0.279	0.140±0.005	0.698
97	22 17 56.6	-59 41 30	RX J2217.8-5941	0.160	0.83±0.06	-0.67±0.04	—	—	0.169	0.005±0.002	0.026
98	22 30 40.3	-39 42 52	PKS 2227-399	0.318	0.55±0.06	-0.10±0.08	0.61±0.01	-0.19±0.08	—	—	—
99	22 42 37.7	-38 45 16	RX J2242.6-3845	0.221	0.65±0.06	-0.70±0.05	—	—	0.117	0.060±0.010	0.333
100	22 45 20.3	-46 52 12	RX J2245.2-4652	0.201	1.60±0.09	-0.70±0.04	1.98±0.02	-0.71±0.05	0.305	0.218±0.007	1.147
101	22 48 41.2	-51 09 53	RX J2248.6-5109	0.102	2.58±0.10	-0.61±0.03	2.41±0.02	-0.53±0.05	—	—	—
102	22 57 39.0	-36 56 07	MS 2254-36	0.039	2.04±0.11	-0.56±0.04	2.29±0.03	-0.61±0.06	—	—	—
103	22 58 45.4	-26 09 14	RX J2258.7-2609	0.076	0.66±0.09	-0.16±0.12	—	—	0.128	0.122±0.008	0.625
104	23 01 36.2	-59 13 20	RX J2301.6-5913	0.149	0.91±0.07	-0.12±0.06	—	—	—	—	—
105	23 01 52.0	-55 08 31	RX J2301.8-5508	0.140	0.90±0.07	-0.63±0.04	0.65±0.01	-0.67±0.07	—	—	—
106	23 04 37.3	-35 01 13	RX J2304.6-3501	0.042	0.61±0.08	-0.47±0.09	0.19±0.01	-0.48±0.10	—	—	—
107	23 12 34.8	-34 04 20	RX J2312.5-3404	0.202	0.43±0.08	-0.20±0.12	—	—	—	—	—
108	23 17 49.9	-44 22 28	RX J2317.8-4422	0.132	0.80±0.08	-0.79±0.05	—	—	0.142	0.072±0.005	0.410
109	23 25 11.8	-32 36 35	RX J2325.2-3236	0.216	0.58±0.10	-0.62±0.11	—	—	0.115	0.085±0.005	0.425
110	23 25 24.2	-38 26 49	IRAS 23226-38	0.036	1.27±0.12	-0.11±0.09	—	—	—	—	—
111	23 43 28.6	-14 55 30	MS 23409-1511	0.137	0.81±0.07	-0.44±0.07	0.89±0.01	-0.46±0.04	—	—	—
112	23 49 24.1	-31 26 03	RX J2349-3126	0.135	0.64±0.06	-0.53±0.06	0.11±0.01	-0.21±0.13	—	—	—
113	23 57 28.0	-30 27 40	AM 2354-304	0.033	0.56±0.06	-0.26±0.07	—	—	—	—	—

¹ WPVS007: Because of the small number of photons no hardness ratio is given.

² IC 3599: Merged event file of ROR 702704 and 702706

³ RX J1624+75: Only upper limits are available (Grupe et al. 1999b)

Table 2. List of observations, RASS and pointed PSPC and HRI. Listed are begin and end of the observing period, the total exposure time, and the ROSAT Observation Request number (ROR)

No.	name	RASS			PSPC-pointed				HRI pointed			
		begin yymmdd.d	end yymmdd.d	T _{obs} s	begin yymmdd.d	end yymmdd.d	T _{obs} s	ROR	begin yymmdd.d	end yymmdd.d	T _{obs} s	ROR
1	Mkn 335	900713.8	900715.2	375	910629.8	910630.8	24337	700101	971220.4	971221.3	11014	601123
2	ESO 242-G8	901125.4	901127.3	238	930604.4	930605.8	6208	701148	951225.5	951225.5	2291	702639
3	WPVS 007	901123.2	901125.4	299	931111.5	931113.5	9691	701527	960613.4	960624.7	19863	702705
4	RX J0057-22	901216.9	901218.5	466	920618.6	920618.7	2961	701141	—	—	—	—
5	QSO 0056-36	901209.4	901211.5	528	—	—	—	—	961221.0	961230.0	2256	702905
6	RX J0100-51	901128.0	901130.2	306	—	—	—	—	960602.1	960625.4	5155	702633
7	RX J0105-14	900712.9	900714.8	579	—	—	—	—	—	—	—	—
8	RX J0117-38	901212.0	901214.4	540	—	—	—	—	—	—	—	—
9	MS 0117-28	901218.8	901220.9	412	911228.5	911229.3	4467	700445	—	—	—	—
10	RX J0128-18	900715.9	910117.0	418	—	—	—	—	—	—	—	—
11	IRAS01267-21	900715.2	910116.2	344	—	—	—	—	960112.4	960112.5	4853	702655
12	RX J0148-27	900715.9	910117.2	504	920609.4	920610.1	6682	701185	—	—	—	—
13	RX J0152-23	901229.5	901231.2	608	—	—	—	—	960101.8	960112.3	4978	702654
14	Mkn 1044	910114.3	910119.3	370	920809.5	920810.5	2836	700792	—	—	—	—
15	Mkn 1048	910119.0	910120.4	382	930809.2	930810.0	6191	701599	960115.8	960115.0	2411	600866
16	RX J0311-20	910122.9	910124.3	319	—	—	—	—	—	—	—	—
17	RX J0319-26	910122.9	910124.3	263	920818.8	920821.3	6823	701052	—	—	—	—
18	RX J0323-49	910102.4	910105.7	745	921222.9	921223.9	5914	701183	960817.7	960819.7	2428	702670
19	ESO 301-G13	910111.4	910114.7	657	—	—	—	—	960102.7	960105.0	3805	702657
20	VCV0331-37	910121.0	910123.1	244	—	—	—	—	970713.3	970713.4	3427	702902
21	RX J0349-47	910113.7	910120.2	421	—	—	—	—	960117.4	960117.5	2049	600869
22	Fair 1116	910124.0	910125.2	167	—	—	—	—	970712.6	970712.6	2754	702903
23	CTS 44	910805.4	910810.8	588	—	—	—	—	—	—	—	—
24	RX J0412-47	910124.0	910125.2	163	—	—	—	—	951230.0	951230.2	5367	702662
25	RX J0426-57	910109.1	910119.3	796	920407.3	920407.8	4094	700034	960816.5	960816.6	4703	702038
26	Fair 303	910122.1	910125.2	290	911220.4	911220.5	2669	800043	—	—	—	—
27	RX J0437-47	900730.6	910812.4	1037	920920.7	920921.8	6142	701184	970922.1	970926.1	23114	400897
28	RX J0439-53	910805.3	910809.8	148	970220.6	970220.7	1370	190537	—	—	—	—
29	H 0439-272	900812.6	900814.6	122	910310.2	910310.3	4955	700035	—	—	—	—
30	1 ES 0614-58	900920.7	901003.2	2792	—	—	—	—	—	—	—	—
31	RX J0859+48	901014.9	901017.0	448	—	—	—	—	—	—	—	—
32	RX J0902-07	901102.5	901104.2	410	—	—	—	—	—	—	—	—
33	Mkn 110	901018.2	901020.0	617	911101.8	911102.8	6013	700262	951016.8	951101.9	30308	702627
34	PG 0953+41	901029.4	901031.3	485	920430.2	920430.4	7014	700526	—	—	—	—
35	RX J1005+43	901030.1	901101.0	686	—	—	—	—	951101.5	951108.4	4711	702656
36	RX J1007+22	901108.4	901110.1	599	—	—	—	—	—	—	—	—
37	CBS 126	901104.1	901105.9	642	—	—	—	—	951030.8	951031.1	3901	702651
38	HS 1019+37	901104.4	901106.3	643	931029.7	931030.2	13510	800491	—	—	—	—
39	Mkn 141	901019.2	901021.9	694	—	—	—	—	961010.4	961010.8	3589	702664
40	Mkn 142	901029.3	901031.5	762	931021.2	931022.6	8427	600624	—	—	—	—

No.	name	RASS				PSPC-pointed				HRI pointed			
		begin yymmdd.d	end yymmdd.d	T _{obs} s	begin yymmdd.d	end yymmdd.d	T _{obs} s	ROR	begin yymmdd.d	end yymmdd.d	T _{obs} s	ROR	
41	RX J1034+39	901106.8	901108.8	525	911118.8	911119.1	4617	700551	—	—	—	—	—
42	RX J1117+65	901025.8	901028.8	874	—	—	—	—	961022.4	961022.4	2169	702892	
43	PG 1115+407	901115.2	901117.3	446	930520.4	930520.8	6489	700801	951114.9	951115.0	3645	702191	
44	Ton 1388	901124.8	901126.5	422	910529.3	910530.2	24294	700228	950528.0	950528.1	1774	701690	
45	EXO 1128+69	901023.1	901026.3	1099	—	—	—	—	—	—	—	—	
46	B2 1128+31	901122.8	901124.4	423	—	—	—	—	—	—	—	—	
47	SBS 1136+579	901106.2	901108.9	491	930530.1	930530.3	5018	800402	—	—	—	—	
48	Z 1136+3412	901123.2	901125.1	422	930518.5	930519.1	2046	201120	—	—	—	—	
49	Was 26	901129.5	901201.3	602	921207.0	921207.5	4889	701149	—	—	—	—	
50	CASG 855	901122.8	901124.3	378	—	—	—	—	—	—	—	—	
51	Mkn 1310	901214.8	901216.5	481	920707.8	920707.9	3341	201367	—	—	—	—	
52	NGC 4051	901121.8	901123.9	506	911116.0	911116.9	28459	700557	950520.5	950520.6	2587	701884	
53	GQ Com	901201.9	901203.8	666	910604.2	910605.2	25991	700232	960621.4	960621.5	4639	702171	
54	RX J1209+32	901130.7	901202.7	210	930523.5	930523.8	2748	701051	—	—	—	—	
55	PG 1211+143	901210.5	901212.3	609	911217.1	911224.7	3803	700018	—	—	—	—	
56	Mkn 766	901203.9	901205.9	525	921208.6	921210.2	6774	701091	960621.7	960621.7	1518	702633	
57	3C 273	901218.9	901220.7	496	911214.3	911215.2	6140	700191	941222.1	941222.1	2088	701961	
58	RX J1231+70	901026.4	901030.2	1005	—	—	—	—	960504.9	960505.7	4285	702652	
59	Mkn 771	901211.9	901213.7	604	911213.3	911228.2	6402	700435	—	—	—	—	
60	CBS 150	901206.7	901208.8	690	920702.3	920702.7	3120	701050	—	—	—	—	
61	MCG+08-23-06	901127.7	901130.1	661	—	—	—	—	—	—	—	—	
62	IC 3599	901209.9	901211.9	658	920630.3	920701.9	5422	701097	960630.5	960702.1	31621	¹	
63	NGC 4593	900715.1	910115.8	180	920714.3	920714.3	1261	701012	960114.9	960116.4	1912	701885	
64	IRAS 1239+33	901207.3	901209.3	707	911215.7	920104.2	19536	600129	—	—	—	—	
65	PG 1244+026	900714.1	900715.3	239	911222.2	911224.8	5486	700020	—	—	—	—	
66	RX J1304+02	901227.9	910117.2	401	—	—	—	—	—	—	—	—	
67	PG 1307+085	900716.2	910117.0	509	920713.5	920719.0	7682	700229	950714.7	950714.9	2950	400625	
68	RX J1314+34	901213.9	901216.1	740	920706.8	920706.8	2526	700802	960108.8	960110.1	5916	702660	
69	RX J1319+52	901129.8	901202.8	714	—	—	—	—	—	—	—	—	
70	PG 1322+659	901110.9	901114.5	810	921130.0	921201.9	8387	700803	—	—	—	—	
71	IRAS 1334+24	910115.3	910116.8	506	920107.7	920114.6	3281	700553	960716.7	960721.8	6207	702625	
72	Ton 730	900716.3	910117.1	592	—	—	—	—	—	—	—	—	
73	RX J1355+56	901202.1	901205.6	829	—	—	—	—	970529.8	970529.9	2577	702897	
74	PG 1402+25	901231.4	910102.6	627	920107.7	920113.3	2692	700226	960114.2	960114.3	4379	702152	
75	RX J1413+70	901104.2	901109.2	501	—	—	—	—	951023.9	951114.3	4140	702659	
76	NGC 5548	910104.1	910117.5	631	921225.4	921225.7	8126	700536	950124.6	950125.1	2260	701950	
77	Q 1421-0013	910119.5	910120.8	442	—	—	—	—	—	—	—	—	
78	Mkn 813	910109.2	910111.1	684	—	—	—	—	—	—	—	—	
79	Mkn 684	910105.8	910118.7	538	—	—	—	—	970719.9	970720.1	2835	702907	
80	Mkn 478	910104.2	910118.0	692	920117.6	920117.8	2354	700559	971224.1	971224.5	9632	704273	

No.	name	RASS			PSPC-pointed					HRI pointed		
		begin yymmdd.d	end yymmdd.d	T _{obs} s	begin yymmdd.d	end yymmdd.d	T _{obs} s	ROR	begin yymmdd.d	end yymmdd.d	T _{obs} s	ROR
81	PG 1448+273	910111.8	910114.1	701	—	—	—	—	—	—	—	—
82	Mkn 841	910124.4	910125.8	451	920120.2	920126.1	16842	700257	950801.0	950808.9	2699	701677
83	HS 1529+56	900714.2	910117.1	1287	—	—	—	—	—	—	—	—
84	Mkn 493	910807.3	910810.0	553	920201.4	920129.6	8038	700096	—	—	—	—
85	Mkn 876	901201.6	901210.8	1906	911123.3	911203.9	6514	700230	—	—	—	—
86	RX J1618+36	900730.6	910803.1	1142	—	—	—	—	960220.9	960222.8	4473	702658
87	KUG 1618+40	900730.3	910812.5	1046	—	—	—	—	—	—	—	—
88	RX J1624+75	901007.4	901015.9	1766	920112.9	920113.8	2923	141829	—	—	—	—
89	PG 1626+554	910114.5	910123.2	1122	930803.5	930804.7	2328	701372	—	—	—	—
90	EXO 1627+401	900801.2	900804.9	1188	930730.2	930730.8	5175	701507	—	—	—	—
91	HS 1702+32	900818.9	910218.1	1117	930803.3	930803.7	11317	800530	—	—	—	—
92	II Zw 136	901111.5	901113.3	562	930529.8	930605.1	8622	701252	951117.2	951117.2	2155	702638
93	RX J2146-30	901031.5	901102.3	475	—	—	—	—	—	—	—	—
94	A 09.25	901104.4	901106.1	342	—	—	—	—	—	—	—	—
95	NGC 7214	901106.6	901108.4	328	920501.1	920502.2	15756	600175	951113.0	951114.8	34040	800848
96	RX J2216-44	901031.6	901102.6	471	—	—	—	—	951108.4	951108.4	57	702650
97	RX J2217-59	901022.5	901024.8	587	—	—	—	—	980415.7	980418.0	9760	601124
98	PKS 2227-399	901106.1	901107.6	425	930530.7	930530.8	3652	701081	—	—	—	—
99	RX J2242-38	901109.1	901110.7	472	—	—	—	—	961201.8	961204.4	756	702895
100	RX J2245-46	901105.2	901107.1	340	921118.9	921128.6	5507	701186	941129.4	941130.8	4515	201870
101	RX J2248-51	901103.1	901104.7	499	931102.3	931103.0	4517	701601	—	—	—	—
102	MS 2254-36	901113.0	901114.3	284	920502.8	920502.9	5514	700554	—	—	—	—
103	RX J2258-26	901118.1	901120.0	143	—	—	—	—	961117.5	961118.4	2538	702909
104	RX J2301-59	901029.8	901101.3	485	—	—	—	—	—	—	—	—
105	RX J2301-55	901102.3	901104.7	541	930518.7	930531.5	8806	701189	—	—	—	—
106	RX J2304-35	901115.3	901117.2	204	921201.7	921204.3	9101	701187	—	—	—	—
107	RX J2312-34	901117.9	901119.0	175	—	—	—	—	—	—	—	—
108	RX J2317-44	901113.0	901114.3	269	—	—	—	—	970507.3	970507.4	3050	702889 ²
109	RX J2325-32	901121.1	901122.1	104	—	—	—	—	961130.7	961130.8	3953	702896
110	IRAS 23226-3	901118.0	901119.2	142	—	—	—	—	—	—	—	—
111	MS 23409-151	901203.1	901204.7	341	921220.7	921221.6	14428	701205	—	—	—	—
112	RX J2349-31	901126.7	901128.7	452	930531.1	930531.3	8148	701190	—	—	—	—
113	AM 2354-304	901129.1	901130.6	446	—	—	—	—	—	—	—	—

¹ IC 3599: Merged event file of ROR 702704 and 702706² RX J2317-44: ROR = 702889h-1, 702889 is empty

Fig. 1 shows that most sources show variability on long timescales of years by factors of about 2-3 (see also Table 1), but do not show dramatic changes in their count rates. However four sources are highly variable in X-rays. Three of these sources are considered to be X-ray transient AGN: RX J1624.9+7554 (Grupe et al. 1999b), WPVS007 (Grupe et al. 1995b), and IC 3599 (Brandt et al. 1995, Grupe et al. 1995a). The other source, RX J2217.9-5941, has changed its count rate between RASS and pointed observations by a factor of more than 30 (Grupe et al. 2000b, and see below). We can exclude line-of-sight Cataclysmic Variables in our Galaxy as the origin of the transience (see discussions in the separate papers of the sources). Four sources have become brighter in their pointed PSPC observation by a factor of more than 2. The sources with the highest count rate ratios are Mkn 771, Mkn 841, NGC 7214, and Mkn 110.

We performed two tests for variability, a χ^2 test for the RASS data (short term behavior) and a check on the amplitude change per unit time for the long term behavior. Fig 2 displays the results of variability tests as a function of the X-ray luminosity in the rest-frame energy 0.2-2.0 keV. In the left panel of Fig. 2 the short term variability of the RASS data is displayed (NGC 4051 and Mkn 766 are off the plot). For objects which have RASS observations that were about half a year apart (see Table 3), only the one with the longest exposure was used. A RASS coverage was typically a few days (see Table 2 for details) with an time increment of 96 minutes (the ROSAT orbit). The reduced χ^2 was calculated from the mean count rate taking the count rate errors into account. We see that there is a slight dependence of the variability strength on luminosity. Low-luminosity sources tend to be slightly more variable than high-luminosity sources. However, Mkn 478 and RX J1304+02, and RX J2217-59 fall off this trend. The two sources with the strongest variability on short timescales are NGC 4051 and Mkn 766, both well-known for their strong variability (see e.g. Peterson et al. 2000 and Leighly et al. 1996). The other two sources with relatively strong variability, RX J1304+02 and RX J2217-59 are ‘new’. On long timescales, RX J1304+02 lacks in further pointed observations and RX J2217-59 is a transient candidate (Grupe et al. 2000b and see below). The X-ray transient AGN do not show unusually strong variability on short timescales.

The long-term behaviour is shown in the right panel of Fig. 2. We also see a slight tendency for low-luminosity sources to be more variable. We took all sources into account for which at least two observations existed that were more than half a year apart. This includes also those sources for which two RASS coverages existed (see Table 3, marked as triangles in Fig. 2). Clearly, in the long-term behaviour, the transients have the highest change in amplitude over time. Two other sources, NGC 4593 and HS1702+32 also show very strong variability on long-timescales. Note that our transient candidate RX J2217.9-

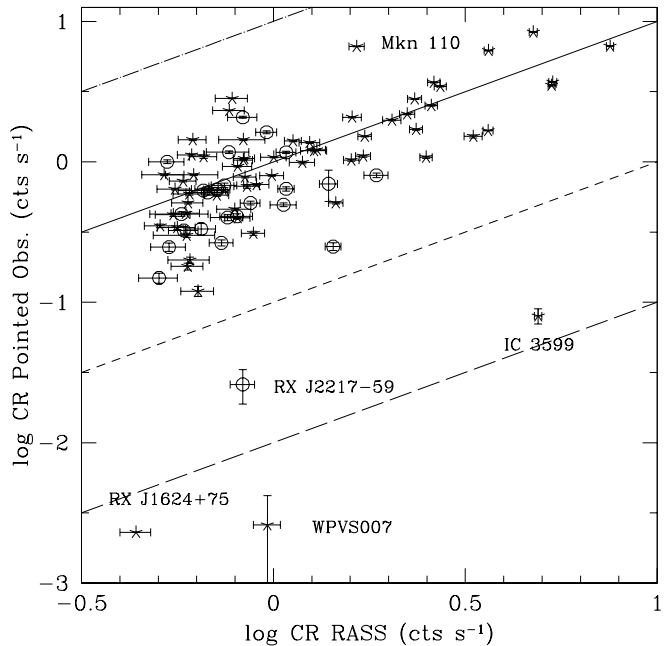


Fig. 1. RASS vs. pointed observation count rate. PSPC observations are marked as stars and HRI observations as open circles. The solid line represents no change between RASS and pointed observation, the dot-dashed line represents to a factor of 10, the short-dashed line to a factor of 0.1, and the long-dashed line to a factor of 0.01. The HRI count rates were converted into PSPC count rates (see section 2)

5941 is the source with the strongest variability between RASS and HRI observation.

Fig. 3 displays the variability strength χ^2/ν (same as in Fig. 2) as a function of the X-ray spectral slope α_x . We found that sources with steep X-ray spectra tend to show stronger variabilities. The dashed lines in Fig. 3 mark the medians of α_x and χ^2/ν without the high variability sources NGC 4051 and Mkn 766 and the source with the steepest X-ray spectrum, WPVS007. Dividing our sample in a steep and flat X-ray spectrum (divided by the median $\alpha_x=1.67$) we find a mean $\chi^2/\nu=1.50$ (with a median of 1.48) for the flat X-ray slope sub-sample and $\chi^2/\nu=2.00$ (median 1.72) for the step X-ray spectrum objects.

3.2. Spectral variability

Fig. 4 shows the hardness ratios of the RASS vs. the pointed PSPC observations. Most sources do not show dramatic spectral changes. Only two objects, RX J2349.3-3126 (see below) and 3C 273, may have varied. Indeed, the difference between the hardness ratios of the RASS and the pointed PSPC observations is small: the mean hardness ratio increased by 0.03. Fig. 5 displays the count rate ratio vs. the difference in the hardness ratios between the RASS and the later pointed PSPC observations. The pur-

Table 3. List of sources that were observed twice during the RASS half a year apart. Observing dates give the beginning of the RASS coverage in yyymmdd, the exposure time T_{exp} is given in s, and the count rate in cts s^{-1} .

#	name	first observation			second observation		
		UT date	T_{exp}	CR	UT date	T_{exp}	CR
10	RX J0128-18	900715	99.4	0.088 ± 0.130	910115	318.5	1.056 ± 0.434
11	IRAS01267-21	900715	210.0	0.724 ± 0.259	910115	133.8	0.837 ± 0.409
12	RX J0148-27	900715	89.4	1.760 ± 0.356	901227	414.1	2.515 ± 0.538
63	NGC 4593	900715	50.1	1.440 ± 0.663	910116	130.2	3.908 ± 0.373
67	PG 1307+085	900716	66.0	0.506 ± 0.264	910115	443.1	0.652 ± 0.261
83	HS 1529+56	900714	583.6	0.963 ± 0.293	901227	703.7	0.639 ± 0.261
87	KUG 1618+40	900730	473.9	0.527 ± 0.247	910810	572.2	0.602 ± 0.331
91	HS 1702+32	900818	810.6	0.345 ± 0.201	910217	306.7	1.130 ± 0.406

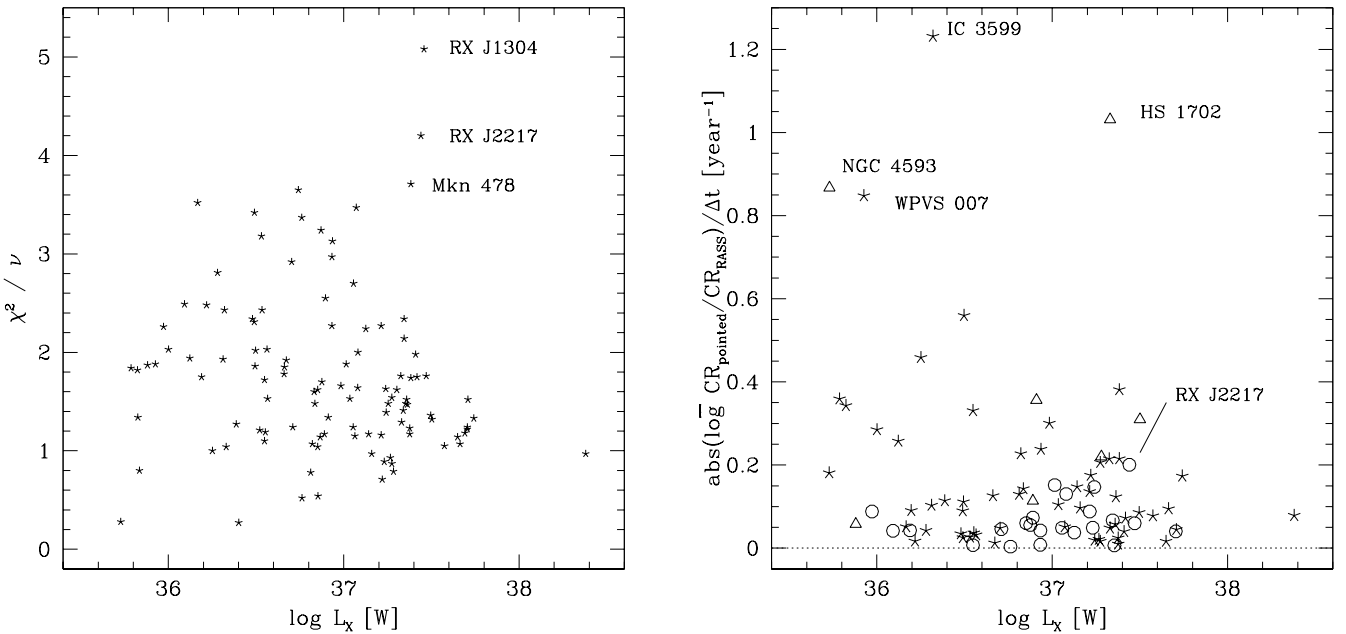


Fig. 2. Variability checks for the soft X-ray AGN sample; the left panel shows the short-term variability in the RASS data and the right panel the long-term variability for all objects for which more than one observation exists (see text). (RASS vs. PSPC observations are marked as stars, RASS vs. HRI as open circles, and RASS vs RASS as open triangles).

pose of this plot is to demonstrate how the sources have changed their spectra with count rate. Obviously, there is no clear correlation between both quantities, the changes going in all possible directions. Spectral changes can also be studied, of course, by using the spectral index α_x . However, the α_x depend on model fitting. We prefer to compare hardness ratios because they are determined directly from the observed counts, and the uncertainties are more simply interpreted. The mean change in hardness ratio for small count rate changes (ratios between 0.8 and 1.2) turns out to be 0.04 ± 0.01 . This might be due to some small losses of hard photons by the off-axis correction for the RASS data as compared to the pointing data, which are usually taken on-axis, and therefore not be an intrinsic property of our sample.

3.3. Spectral analysis

Table 4 lists the spectral analysis of the RASS and pointed PSPC data. For the power-law fits to the RASS and pointed PSPC data with the absorption parameter N_H fixed to the Galactic value, the X-ray fluxes are given in the restframe ROSAT energy range between 0.2-2.0 keV.

The mean X-ray slope of the RASS observation using a power-law fit with fixed N_H is $\alpha_x=1.81$ with a median of 1.67. This is slightly flatter than we found for our original sample ($\langle \alpha_x \rangle = 2.10$; Grupe et al. 1998a). The mean X-ray luminosity derived from this spectral model is $\log L_X=36.87$ [W] with a median of 36.91. The object with the highest luminosity is 3C 273 ($\log L_X=38.4$). Dividing the sample into low and high luminosity subsamples using

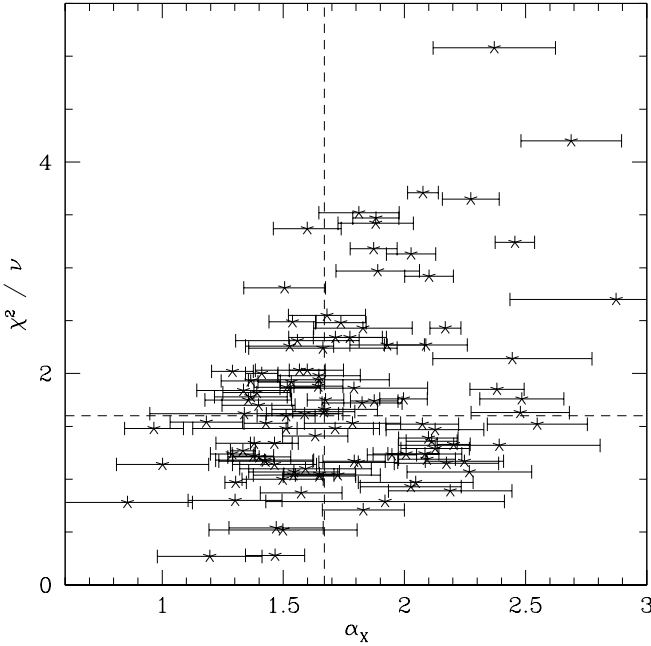


Fig. 3. Short-term χ^2 variability vs. X-ray spectral slope α_x . The dashed lines mark the medians in α_x and χ^2/ν . Three objects are off the plot, NGC 4051, Mkn 766 and WPVS007 (with positions at 1.62, 18.54; 1.11, 8.86; and 8.70, 1.88 respectively).

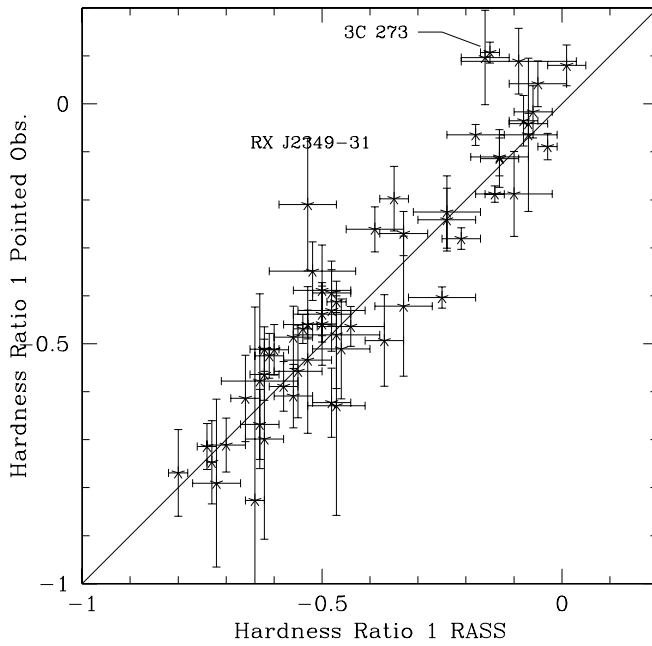


Fig. 4. RASS vs. pointed observation hardness ratio

the median of $\log L_X$ as the borderline, we find a difference in the distribution of the X-ray slope α_x . The low-luminosity sub-sample has a mean of $\langle \alpha_x \rangle = 1.61$ (me-

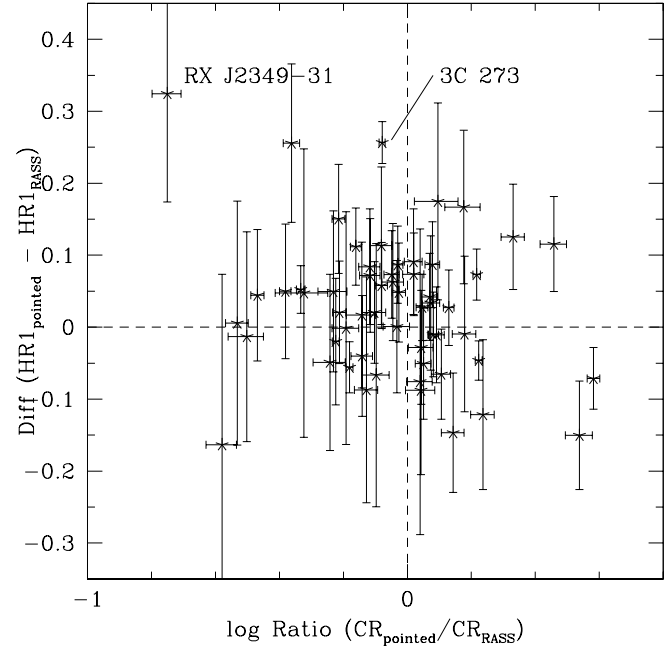


Fig. 5. Ratio of the count rates of pointed PSPC and RASS vs. the difference between their HR1. The transients IC 3599 and WPVS007 fall outside the boundaries of the plot.

dian=1.54), the high-luminosity sub-sample $\langle \alpha_x \rangle = 1.89$ (median=1.92).

3.4. Individual X-ray transient AGN

Here, we present new results of HRI observations of the X-ray transient AGN IC3599 and WPVS007. We briefly review the other most recently discovered transients, RX J1624.9+7554 and RX J2217.9-5941.

3.4.1. IC 3599

The Seyfert 2 galaxy IC 3599 was one of the brightest AGN of our sample during the RASS ($4.90 \text{ PSPC cts s}^{-1}$) and was seen even with the Wide Field Camera (WFC) that was attached to ROSAT (Pounds et al. 1993, Edelson et al. 1999). It became fainter in pointed PSPC observations in the following years by a factor of about 100 (see Grupe et al. 1995a, Brandt et al. 1995). We made two ROSAT HRI observations between 1996-06-30 and 1996-07-02 to monitor its long term behaviour. In order to get better photon statistics on the source, both event files were merged into one. From this merged event file with a total exposure time of 31621 s an HRI count rate of $4.62 \pm 0.49 \cdot 10^{-3}$ was measured, which corresponds to $0.025 \text{ PSPC cts s}^{-1}$ (see Table 1) and an X-ray luminosity in the 0.2-2.0 keV band of $\log L_X = 33.6$. Fig. 6 displays the long-term light curve. IC 3599 has shown a response in its optical emission line spectrum. Shortly after the RASS,

highly ionized iron lines like FeXIV were observed (see Brandt et al. 1995). A year later, these lines disappeared but other lower ionized iron lines like FeVII and FeX appeared (Grupe et al. 1995a).

Table 4. Spectral analysis of the RASS and pointed PSPC observations. The absorption parameters $N_{\text{H,fit}}$ and $N_{\text{H,gal}}$ are given in units of $10^{20} \text{ cm s}^{-1}$ and the X-ray flux F_X in Watts m $^{-2}$ in the rest-frame energy band between 0.2-2.0 keV.

No.	name	RASS				PSPC-pointed					
		$N_{\text{H,fit}}$	α_x	χ^2/ν	$N_{\text{H,gal}}$	α_x	χ^2/ν	$\log F_X$	α_x	χ^2/ν	$\log F_X$
1	Mkn 335	4.49±1.36	2.29±0.29	15/19	3.96	2.10±0.10	16/20	-13.40	2.13±0.01	233/178	-13.47
2	ESO 242-G8	0.70±1.14	1.13±0.66	15/10	1.48	1.56±0.26	17/11	-14.31	1.64±0.05	53/56	-14.45
3	WPVS 007	0.68±0.71	3.10±0.99	5.4/13	2.82	8.70±1.75	8.9/14	-14.27	—	—	—
4	RX J0057-22	1.37±0.51	1.82±0.27	25/25	1.48	1.89±0.10	25/26	-13.77	1.99±0.03	78/93	-13.63
5	QSO 0056-36	1.73±1.19	1.62±0.51	29/22	1.94	1.72±0.16	29/23	-14.29	—	—	—
6	RX J0100-51	2.49±1.59	1.75±0.52	16/18	2.42	1.73±0.18	16/19	-13.99	—	—	—
7	RX J0105-14	2.34±0.91	1.53±0.30	30/19	1.77	1.29±0.09	32/20	-13.89	—	—	—
8	RX J0117-38	2.82±1.35	2.41±0.44	3.9/9	2.08	2.09±0.15	5.4/10	-14.18	—	—	—
9	MS 0117-28	2.13±1.56	2.51±0.66	6.8/13	1.65	2.27±0.26	7.2/14	-14.54	2.70±0.12	28/31	-14.46
10	RX J0128-18	1.82±1.31	1.64±0.55	14/19	1.62	1.55±0.17	14/20	-14.26	—	—	—
11	IRAS01267-21	1.51±1.26	1.55±0.62	14/15	1.28	1.43±0.19	14/16	-14.29	—	—	—
12	RX J0148-27	2.54±0.82	2.62±0.30	21/22	1.50	2.12±0.11	30/23	-13.90	1.88±0.03	178/110	-13.90
13	RX J0152-23	1.25±0.68	1.75±0.39	17/13	1.10	1.67±0.13	17/14	-14.26	—	—	—
14	Mkn 1044	3.99±1.38	2.04±0.32	21/17	3.16	1.74±0.10	22/18	-13.52	1.75±0.03	144/118	-13.52
15	Mkn 1048	3.18±1.62	1.67±0.43	13/9	2.83	1.53±0.14	13/10	-13.84	1.51±0.03	181/140	-13.77
16	RX J0311-20	1.02±1.15	8.63±0.56	23/17	2.37	1.47±0.19	27/18	-14.09	—	—	—
17	RX J0319-26	0.52±1.09	1.39±0.73	6.3/7	1.32	1.79±0.31	7.1/8	-14.55	1.42±0.03	88/83	-14.23
18	RX J0323-49	2.45±0.85	2.35±0.29	36/21	1.72	2.03±0.10	39/22	-14.02	1.83±0.05	79/55	-14.39
19	ESO 301-G13	1.66±0.91	1.75±0.41	20/11	2.19	2.01±0.14	21/12	-14.09	—	—	—
20	VCV0331-37	1.48±1.76	1.51±0.89	6.0/7	1.63	1.59±0.27	6.0/8	-14.32	—	—	—
21	RX J0349-47	0.78±0.80	2.04±0.58	13/12	1.44	2.45±0.33	15/13	-14.75	—	—	—
22	Fair 1116	2.43±1.58	1.87±0.53	20/17	3.84	2.48±0.20	22/18	-13.56	—	—	—
23	CTS 44	1.08±0.39	1.33±0.20	27/35	1.24	1.41±0.07	27/36	-13.66	—	—	—
24	RX J0412-47	0.82±1.39	1.36±0.81	2.8/6	1.42	1.66±0.31	3.2/7	-14.34	—	—	—
25	RX J0426-57	1.12±0.31	1.62±0.20	44/30	2.25	2.20±0.07	70/31	-13.53	2.10±0.02	333/154	-13.19
26	Fair 303	1.69±1.12	1.89±0.51	13/20	0.99	1.51±0.17	15/21	-14.19	1.31±0.05	58/53	-14.24
27	RX J0437-47	1.07±0.46	1.74±0.31	28/21	1.69	2.09±0.12	33/22	-14.14	1.93±0.03	184/91	-13.96
28	RX J0439-53	1.35±1.85	2.28±1.04	3.1/5	1.55	2.39±0.42	32/6	-14.44	—	—	—
29	H 0439-272	1.98±3.99	1.30±1.57	6.8/3	2.43	1.51±0.39	6.8/4	-14.26	1.27±0.04	90/88	-14.04
30	1 ES 0614-58	4.37±1.00	2.38±0.23	20/30	4.60	2.46±0.08	20/31	-13.90	—	—	—
31	RX J0859+48	1.99±1.46	1.44±0.57	16/17	2.05	1.46±0.17	16/18	-14.22	—	—	—
32	RX J0902-07	3.54±2.45	2.12±0.62	16/13	3.68	2.17±0.22	16/14	-14.08	—	—	—
33	Mkn 110	1.47±0.64	1.25±0.30	13/21	1.56	1.29±0.09	13/22	-13.86	1.47±0.01	290/182	-13.26
34	PG 0953+41	2.30±1.26	2.26±0.46	7.6/8	1.14	1.65±0.15	13/9	-14.34	1.55±0.04	47/73	-14.28
35	RX J1005+43	1.65±0.96	2.15±0.46	9.4/9	1.08	1.81±0.16	11/10	-14.49	—	—	—
36	RX J1007+22	6.20±2.79	2.91±0.54	15/21	2.69	1.68±0.16	24/22	-14.19	—	—	—
37	CBS 126	1.36±0.62	1.62±0.33	18/19	1.41	1.65±0.10	18/20	-14.03	—	—	—
38	HS 1019+37	1.32±0.95	9.83±0.43	12/9	1.28	0.98±0.12	12/10	-14.23	—	—	—
39	Mkn 141	1.68±1.30	1.84±0.58	15/16	1.07	1.53±0.18	16/17	-14.54	—	—	—
40	Mkn 142	1.61±0.55	2.10±0.27	34/26	1.18	1.88±0.10	36/27	-14.04	1.77±0.03	139/85	-14.20

No.	name	RASS				PSPC-pointed					
		$N_{\text{H,fit}}$	α_x	χ^2/ν	$N_{\text{H,gal}}$	α_x	χ^2/ν	log Fx	α_x	χ^2/ν	logFx
41	RX J1034+39	2.71±0.79	3.00±0.31	13/25	1.50	2.38±0.11	26/26	-13.85	2.42±0.03	376/91	-13.67
42	RX J1117+65	1.95±1.10	2.50±0.49	6.9/9	0.91	1.89±0.17	12/10	-14.62	—	—	—
43	PG 1115+407	1.42±1.27	1.81±0.66	13/13	1.93	2.05±0.24	13/14	-14.43	1.98±0.06	49/44	-14.53
44	Ton 1388	1.14±0.91	1.61±0.57	11/7	1.22	1.65±0.17	11/8	-14.29	1.62±0.02	193/149	-14.12
45	EXO 1128+69	1.12±0.40	1.49±0.22	42/34	1.34	1.60±0.07	42/35	-13.97	—	—	—
46	B2 1128+31	2.61±2.08	1.59±0.66	12/12	2.22	1.43±0.20	12/13	-14.38	—	—	—
47	SBS 1136+579	1.42±1.22	1.77±0.63	18/16	1.00	1.54±0.19	18/17	-14.54	1.58±0.19	4.1/6	-15.38
48	Z 1136+3412	1.81±1.24	1.72±0.52	19/19	2.04	1.81±0.17	19/20	-14.14	1.81±0.09	22/24	-14.36
49	Was 26	2.75±0.97	1.69±0.29	22/20	2.10	1.43±0.09	24/21	-13.82	1.43±0.03	121/92	-13.98
50	CASG 855	1.64±1.03	1.33±0.47	9.4/9	1.80	1.40±0.13	9.5/10	-13.95	—	—	—
51	Mkn 1310	2.31±1.37	1.35±0.47	14/8	2.43	1.39±0.14	14/9	-14.01	1.13±0.12	18/14	-14.71
52	NGC 4051	2.23±0.59	2.02±0.22	31/36	1.37	1.62±0.07	41/37	-13.60	1.65±0.01	361/177	-13.92
53	GQ Com	1.94±1.23	1.30±0.50	27/21	1.66	1.18±0.15	27/22	-14.37	1.20±0.02	131/140	-14.40
54	RX J1209+32	4.34±4.52	3.18±1.18	2.7/5	0.00	0.86±0.27	19/6	-14.73	1.09±0.09	36/20	-14.98
55	PG 1211+143	3.04±1.02	2.12±0.29	22/21	2.75	2.00±0.09	2.2/22	-13.74	1.82±0.04	84/78	-13.86
56	Mkn 766	3.40±0.64	1.77±0.16	19/29	1.69	1.11±0.05	57/30	-13.31	1.28±0.01	474/171	-13.48
57	3C 273	1.58±0.34	1.21±0.16	56/42	1.79	1.30±0.05	57/43	-13.23	1.00±0.01	234/200	-13.18
58	RX J1231+70	1.95±0.75	1.49±0.29	16/22	1.67	1.38±0.08	16/23	-14.12	—	—	—
59	Mkn 771	3.64±1.88	2.46±0.51	19/19	2.05	1.83±0.16	24/20	-14.32	1.64±0.03	123/126	-13.87
60	CBS 150	3.41±2.01	2.94±0.62	20/18	1.44	2.13±0.20	26/19	-14.71	1.89±0.09	23/27	-14.60
61	MCG+08-23-06	1.36±1.09	1.36±0.53	19/19	1.40	1.38±0.16	19/20	-14.37	—	—	—
62	IC 3599	4.04±0.71	3.37±0.21	55/32	1.34	2.17±0.06	169/33	-13.60	2.61±0.35	11/6	-15.59
63	NGC 4593	1.57±0.94	1.19±0.42	15/11	2.28	1.47±0.12	16/12	-13.46	1.19±0.05	54/54	-13.78
64	IRAS 1239+33	2.74±1.38	2.02±0.42	19/11	1.35	1.37±0.12	25/12	-14.24	1.28±0.03	195/98	-14.43
65	PG 1244+026	1.08±0.99	1.44±0.53	21/16	1.75	1.79±0.20	22/17	-14.06	1.85±0.03	118/83	-14.02
66	RX J1304+02	1.50±1.13	2.26±0.59	18/18	1.74	2.38±0.25	18/19	-14.44	—	—	—
67	PG 1307+085	2.75±1.85	1.87±0.55	8.8/17	2.05	1.58±0.17	8.9/18	-14.32	1.58±0.04	86/80	-14.24
68	RX J1314+34	1.93±1.08	2.35±0.45	9.5/9	0.99	1.88±0.16	13/10	-14.51	1.76±0.14	24/11	-14.87
69	RX J1319+52	2.04±1.12	2.06±0.44	4.5/9	1.16	1.60±0.14	8.0/10	-14.41	—	—	—
70	PG 1322+659	1.32±0.77	1.74±0.42	5.5/10	2.01	2.07±0.15	7.5/11	-14.30	1.81±0.04	64/73	-14.27
71	IRAS 1334+24	1.36±0.50	2.01±0.27	20/25	1.12	1.88±0.10	21/26	-13.92	1.83±0.05	57/53	-14.20
72	Ton 730	1.29±0.99	1.96±0.57	13/16	1.05	1.83±0.20	13/17	-14.59	—	—	—
73	RX J1355+56	1.85±0.92	2.31±0.42	15/10	1.15	1.93±0.15	18/11	-14.47	—	—	—
74	PG 1402+25	1.52±1.01	1.85±0.50	4.0/7	1.48	1.83±0.17	4.0/8	-14.42	1.91±0.06	51/49	-14.12
75	RX J1413+70	1.15±0.98	1.07±0.47	13/23	1.93	1.40±0.15	14/24	-14.20	—	—	—
76	NGC 5548	1.47±0.38	1.13±0.17	47/30	1.93	1.33±0.05	52/31	-13.35	1.50±0.01	324/201	-13.10
77	Q 1421-0013	5.99±3.21	2.71±0.62	17/14	2.97	1.72±0.19	22/15	-14.23	—	—	—
78	Mkn 813	1.29±0.87	1.11±0.42	8.2/10	2.54	1.64±0.14	13/11	-14.12	—	—	—
79	Mkn 684	1.68±1.38	1.44±0.61	12/15	1.50	1.36±0.18	13/16	-14.40	—	—	—
80	Mkn 478	1.27±0.26	2.22±0.16	20/32	1.04	2.08±0.06	24/33	-13.64	2.18±0.05	68/54	-13.95

No.	name	RASS				PSPC-pointed					comments
		$N_{\text{H,fit}}$	α_x	χ^2/ν	$N_{\text{H,gal}}$	α_x	χ^2/ν	log Fx	α_x	χ^2/ν	
81	PG 1448+273	4.52±1.70	2.13±0.37	6.6/11	2.71	1.52±0.12	13/12	-14.05	—	—	—
82	Mkn 841	2.48±1.60	1.61±0.52	23/19	2.24	1.50±0.17	23/20	-14.13	1.42±0.01	220/190	-13.61
83	HS 1529+56	1.77±0.73	1.78±0.32	20/18	1.15	1.46±0.10	24/19	-14.32	—	—	—
84	Mkn 493	1.51±1.33	1.26±0.62	9.0/16	2.22	1.57±0.18	9.7/17	-14.28	1.60±0.04	55/66	-14.39
85	Mkn 876	2.68±0.79	1.57±0.24	28/30	2.95	1.67±0.08	28/31	-14.03	1.62±0.03	143/124	-13.86
86	RX J1618+36	1.57±0.67	1.69±0.31	15/19	1.26	1.54±0.10	15/20	-14.24	—	—	—
87	KUG 1618+40	1.63±0.97	1.87±0.45	14/10	0.96	1.52±0.14	16/11	-14.50	—	—	—
88	RX J1624+75	5.65±1.77	2.89±0.37	14/15	3.87	2.28±0.12	19/16	-14.14	—	—	—
89	PG 1626+554	1.23±0.76	1.42±0.38	17/12	1.99	1.79±0.13	20/13	-14.33	2.02±0.06	71/50	-14.00
90	EXO 1627+401	0.71±0.38	2.15±0.37	7.0/15	0.84	2.25±0.16	7.4/16	-14.65	2.16±0.05	75/53	-14.31
91	HS 1702+32	2.12±1.03	1.99±0.39	9.1/11	2.42	2.13±0.14	9.4/12	-14.31	2.43±0.05	44/57	-14.27
92	II Zw 136	2.53±1.10	1.37±0.34	16/15	4.65	2.10±0.12	26/16	-13.60	2.08±0.03	181/145	-13.57
93	RX J2146-30	2.49±1.60	1.66±0.51	22/21	2.31	1.59±0.16	22/22	-14.15	—	—	—
94	A 09.25	2.03±1.31	1.63±0.50	8.2/20	1.47	1.37±0.15	9.0/21	-14.14	—	—	—
95	NGC 7214	0.95±1.24	1.02±0.63	16/14	1.62	1.34±0.20	16/15	-14.21	1.68±0.01	291/181	-13.65
96	RX J2216-44	1.23±0.64	1.98±0.38	1.1/12	2.17	2.48±0.17	16/13	-14.02	—	—	—
97	RX J2217-59	1.36±0.84	2.08±0.46	7.3/8	2.58	2.69±0.21	12/9	-14.18	—	—	—
98	PKS 2227-399	0.63±1.03	0.72±0.55	8.2/13	1.20	1.00±0.19	9.1/14	-14.50	1.15±0.05	48/56	-14.31
99	RX J2242-38	2.69±1.81	2.92±0.70	16/16	1.18	2.19±0.26	2.0/17	-14.64	—	—	—
100	RX J2245-46	0.61±0.49	1.71±0.35	21/10	1.95	2.55±0.21	33/11	-14.09	2.59±0.04	348/82	-13.75
101	RX J2248-51	0.88±0.39	1.72±0.24	26/24	1.27	1.95±0.10	28/25	-13.88	1.76±0.03	160/112	-13.77
102	MS 2254-36	1.27±0.75	1.84±0.43	30/11	1.15	1.78±0.15	30/12	-13.97	1.83±0.04	68/68	-14.16
103	RX J2258-26	3.89±4.23	2.11±0.98	6.1/5	2.11	1.50±0.31	6.6/6	-14.25	—	—	—
104	RX J2301-59	1.40±1.04	1.10±0.48	7.0/8	2.69	1.65±0.15	11/9	-14.00	—	—	—
105	RX J2301-55	1.50±0.88	2.04±0.45	9.6/9	1.54	2.09±0.17	9.6/10	-14.30	2.22±0.04	101/64	-14.32
106	RX J2304-35	1.43±2.01	1.63±1.01	4.7/7	1.47	1.65±0.29	4.7/8	-14.39	1.73±0.06	35/40	-14.86
107	RX J2312-34	0.71±2.14	0.78±1.13	3.5/3	1.80	1.34±0.39	4.3/4	-14.50	—	—	—
108	RX J2317-44	1.30±1.23	2.50±0.80	10/10	1.89	2.87±0.44	11/11	-14.41	—	—	—
109	RX J2325-32	1.50±2.90	2.01±1.44	0.8/2	1.33	1.92±0.49	0.8/3	-14.57	—	—	—
110	IRAS 23226-3	1.99±2.07	1.38±0.80	8.0/9	1.59	1.20±0.22	8.2/10	-13.98	—	—	—
111	MS 23409-151	3.65±2.29	2.60±0.63	16/14	2.20	2.03±0.21	18/15	-14.23	2.09±0.02	139/118	-14.03
112	RX J2349-31	1.02±1.01	1.55±0.57	18/14	1.23	1.67±0.22	18/15	-14.50	1.17±0.07	26/25	-15.06
113	AM 2354-304	1.55±1.41	1.39±0.68	9.5/14	1.37	1.30±0.19	9.6/15	-14.39	—	—	—

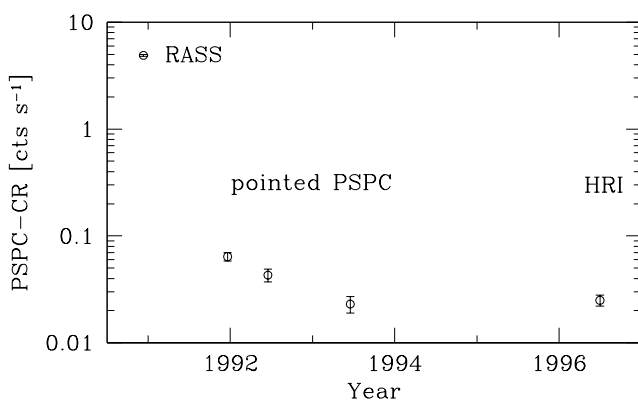


Fig. 6. Long-term light curve of IC3599. The HRI count rate was converted into a PSPC count rate (see Sect. 2).

Monitoring this object in the optical until now shows that these lines are slowly fading. The interpretation of the X-ray outburst in IC 3599 is that it is the result of disk instabilities or tidal disruption of a star by the central black hole (see Brandt et al. 1995 and Grupe et al. 1995a). A similar outburst event has been reported in the galaxy NGC 5905 (Komossa & Bade 1999).

3.4.2. WPVS007

The Narrow-line Seyfert 1 galaxy WPVS007 was the softest AGN detected during the RASS (Grupe et al. 1995b) and it was bright (about 1 cts s^{-1}). Like IC 3599 it was one of a few AGN that were seen during the WFC all-sky survey (Edelson et al. 1999). After the RASS it was observed three years later by the ROSAT PSPC and was practically ‘turned-off’. In the following years we monitored the source four times (see Table 5) using the ROSAT HRI. In two of these observations WPVS007 was detected again (ROR 702705 and 702923). For the other two only upper limits can be given. Fig. 7 shows the new long-term light curve of WPVS007. The HRI count rates of WPVS007 convert to about $\log L_X = 31$ [W]. Like IC 3599 we monitored WPVS007’s optical spectrum over several years. So far we not detected any change in the optical spectrum. A possible interpretation of the transience in WPVS007 is that the temperature of the Comptonization layer above the disk that scatters the thermal UV disk photons into the soft X-ray range, changed. A lower temperature caused a shift of the EUV bump spectrum out of the ROSAT energy range of 0.1–2.4 keV. This explains why the bolometric luminosity changed by a factor of 2 but the PSPC count rate decreased by a factor of 400 (Grupe et al. 1995b). It is also interesting to note that WPVS007 was detected by the HRI considering that no hard photons above 0.5 keV were detected in the RASS observation⁴.

⁴ The HRI has a lower efficiency in soft X-rays than the PSPC

Table 5. Pointed HRI observations of WPVS007. The UT observing dates are given as yyymmdd, the exposure time is in s, the HRI count rate in units of $10^{-4} \text{ HRI cts s}^{-1}$, and the converted PSPC count rate in units of $10^{-3} \text{ PSPC cts s}^{-1}$. 3σ Upper limits are marked as (u.l.).

#	ROR	obs. date	T _{obs}	HRI CR	PSPC CR
1	702703	951118	15994	4.04 (u.l.)	3.22
2	702705	960613	19863	5.14 ± 3.48	4.10
3	702923	971110	10851	4.61 ± 4.33	3.68
4	702921	971206	9976	5.20 (u.l)	4.16
	all	—	56684	5.29 ± 2.00	4.22

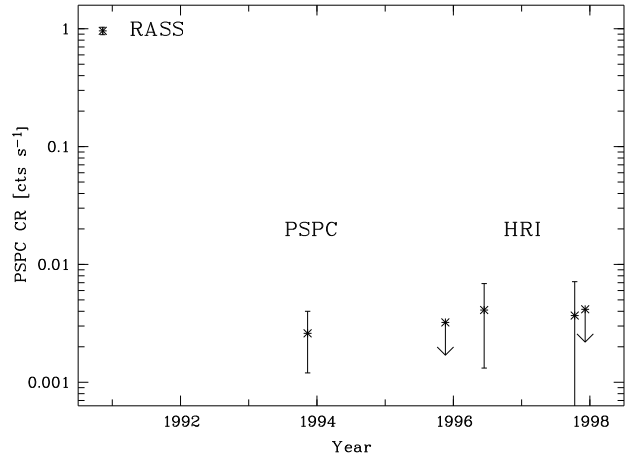


Fig. 7. Long-term light curve of WPVS007. The downwards arrows mark the upper limits of the HRI observations converted into PSPC counts (see Sect. 2).

3.4.3. RX J1624.9+7554

This X-ray transient was discovered in a non-active spiral galaxy (Grupe et al. 1999b). Between the RASS and the pointed PSPC observations years later the object vanished completely in X-rays. Because this source is in its normal state a non-active galaxy, it is most likely that its X-ray outburst was caused by a tidal disruption of a star by the central black hole. Komossa and Greiner (1999) and most recently Greiner et al. (2000) also reported about other X-ray outbursts in a non-active galaxies.

3.4.4. RX J2217.9–5941

This Narrow-line Seyfert 1 galaxy has shown a decrease in its count rate by a factor of about 30 between the RASS and its last HRI observation in 1998 (Grupe et al. 2000, in prep.). It is not yet clear if this is a real transient source, which means the count rate is still decreasing until today, or if it was observed in its ‘low-state’ in both HRI observations in 1997 and 1998. The RASS light curve shows a decline in count rate by a factor of approximately 15

in about two days. However, the HRI count rates do not show strong variability over their four day coverage.

3.4.5. RX J2349.3–3126

RX J2349.3–3126 is the only source in the current sample that has shown a significant change in its X-ray spectrum between the RASS and its pointed PSPC observation two and a half years later. Its hardness ratio has changed from -0.53 ± 0.06 during the RASS to -0.21 ± 0.13 in the pointed observation (Table 1). It also showed a decrease in its mean count rate between the RASS and the pointed observation by a factor of about 6. RX J2349.3–3126 seems to show large amplitude variations only over long time scales. During the RASS coverage the source doubled its count rate in about two days. During the pointed PSPC observation the source remained almost constant over about 6 hours.

Optically, RX J2349.3–3126 is a Seyfert 1 galaxy with very broad emission lines ($\text{FWHM}(\text{H}\beta) = 7715 \text{ km s}^{-1}$; Grupe et al. 1999a). An R-image taken with the ESO/MPG 2.2m telescope at La Silla besides the very bright nucleus displays several bright spots, and tidal tails. So this AGN may be fueled by a merger.

4. Discussion

4.1. X-ray transient AGN

Why are there no ‘turn-ons’ among the sources of our sample? This is a selection effect due to the definition of our sample. Because our sample is chosen to include only sources that were bright during the RASS, we will be biased against sources that were faint then but have since brightened, but we include sources that have since become fainter – sometimes much fainter – than our original count rate limit. For obvious reasons, only the brightest sources were re-observed in later pointed observations. Fainter RASS sources can be seen only serendipitously brighter in pointed observations. Because of the much smaller coverage of the sky in the pointed observations (15% PSPC, 2% HRI; Voges, private communications) there is not much chance to detect a transient in its ‘high’ state. So far only one AGN has been reported being faint in the RASS and bright in a later pointed PSPC observation, RX J1242.6–1119 (Komossa & Greiner 1999).

What causes transience in AGN? The most common explanation of X-ray transience in AGN is a sudden increase of the accretion rate. This could be the result of either accretion disk instabilities, or even the tidal disruption of a star as has been suggested by Rees (1990). While in the Seyfert 2 galaxy IC 3599 both accretion disk instabilities or a tidal disruption of a star might cause the X-ray outburst (Brandt et al. 1995, Grupe et al. 1995a) in non active galaxies like RX J1624.9+7554, RX J1242.6–1119, NGC 5905 (Komossa & Bade 1999) or RX J1420.4+5334

(Greiner et al. 2000) tidal disruption seems to be the more likely explanation. In the case of the X-ray transient WPVS007, Grupe et al. (1995b) discussed the possibility of a temperature change in the Comptonization layer above the disk as an alternative explanation. A lower temperature of this layer would shift the soft X-ray spectrum out of the ROSAT PSPC energy window (0.1–2.4 keV) and would mimic a dramatic change in the X-ray/Big Blue Bump flux.

Converting the HRI count rates of the two transients IC 3599 and WPVS007 into X-ray fluxes shows that they now have typical X-ray luminosities of a normal galaxy (about $\log L_X = 33$ [W]). In both cases, we can consider this as their pre-outburst/transient luminosities.

4.2. X-ray variability

We find that low-luminosity objects have a higher probability of being found to be variable than the high-luminosity ones (Fig. 2). This result is not as prominent as in the samples of Boller et al. (1996) and Leighly (1999a,b). The reason is that their samples stretch over 7 and 5 orders in luminosity while ours only stretches over ≈ 2 orders. However, in our Principal Component Analysis on our original sample (Grupe et al. 1998a, 1999a) we found this result as a part of the Eigenvector 1 relationship. There are two explanations for the dependence of the variability on luminosity: a) the size of the Black Hole/AGN engine, and b) the number of the X-ray emitting regions (see discussion in Leighly 1999a). The χ^2/ν test for the short-term variability in the RASS data is a robust test. It does not take the length of the observation into account. However, the RASS coverages are usually in the order of days and therefore comparable. Only for a few sources the RASS observations were split into two parts half a year apart. We should mention that the result of the distribution of the variability seen in Fig. 2 is smeared out when the excess variance (e.g. Nandra et al. 1997, Leighly 1999a) is used instead if χ^2/ν .

The comparison of the long-term variability (right panel of Fig 2) is more complicated. The time gaps between RASS and pointed observation can vary from source to source between half a year up to 8 years. This is the reason why the HRI data points suggest less variability than the PSPC data, because they have been observed later than the PSPC. The only way to check out the long term variability of a large sample of AGN is repeated monitoring of the sky like it is performed for example by RXTE’s All-Sky Monitor.

Fig. 3 in Leighly 1999a shows that NLS1 are more variable than Broad-line Seyfert 1s. In our sample a large percentage are NLS1 (Grupe et al. 1999a, Grupe et al. 2001 in prep). NLS1 are also objects that have the steepest X-ray spectra (Boller et al. 1996, Grupe et al. 1998a). Therefore we checked for a relation between α_x and the strength of the variability. This is what we find for the

short-term variability throughout the sample: objects with steeper X-ray spectra (preferentially NLS1) show stronger variability than those with flatter X-ray spectra (see Fig. 3). This is in agreement with the findings of Green et al. (1993) where ‘sources with steeper energy spectra have higher normalized variability amplitudes’.

In principle, the same intrinsic processes that apply to X-ray transience (changes in the accretion rate or the disk temperature) also apply to the normal variability, but on a much lower level. In cases of very rapid variability, such as found in IRAS13224–3809 (Boller et al. 1997), relativistic and Doppler boosting and gravitational lensing effects (see Boller et al. 1997, Leighly 1999a) have to be taken into account. The variability will be stronger amplified in steep X-ray sources.

Another alternative explanation of variability is a change in the cold and warm absorber column densities and their ionization states (e.g. Abrassart & Czerny 2000, Komossa & Meerschweinchen 2000).

We have shown that ROSAT with its All-Sky Survey and the later pointed observations was a well suited experiment to detect X-ray transient sources and to monitor the long-term behaviour of AGN. The best way to find more transients would be to perform all-sky surveys repeatedly.

Acknowledgements. We thank Drs Bev Wills, Mario Gliozzi, Wolfgang Voges, Stefanie Komossa, and Joachim Trümper for useful suggestions and discussions. We also want to thank our referee, Prof. Dr. A. Lawrence for his comments on the manuscript and valuable information on additional references. This research has made use of the NASA/IPAC Extragalactic Database (NED) which is operated by the Jet Propulsion Laboratory, Caltech, under contract with the National Aeronautics and Space Administration. The ROSAT project is supported by the Bundesministerium für Bildung, Wissenschaft, Forschung und Technologie (BMBF) and the Max-Planck-Gesellschaft.

This paper can be retrieved via WWW:
<http://www.xray.mpe.mpg.de/~dgrupe/research/refereed.html>

References

- Abrassart A., Czerny B., 2000, A&A 356, 475 /bibitem Barr P., Mushotzky R.F., 1986, Nature 330, 421
 Boller Th., Brandt W.N., Fink H.H., 1996, A&A 305, 53
 Boller Th., Brandt W.N., Fabian A.C., Fink H.H., 1997, MNRAS 289, 393
 Boroson T.A., Green R.F., 1992, ApJS 80, 109
 Brandt W.N., Pounds K.A., Fink H.H., 1995, MNRAS 273, L47
 Brandt W.N., Boller Th., Fabian A.C., Ruszkowski M., 1999, MNRAS 303, L53
 Córdova F.A., Kartje J.F., Thompson R.J., et al., 1992, ApJS 81, 661
 Dickey J.M., Lockman F.J., 1990, ARA&Astrophys. 28, 215
 Edelson R., Vaughan S., Warwick R., Puchnarewicz E., George I., 1999, MNRAS 307, 91
 Green A.R., McHardy I.M., Lehto H.J., 1993, MNRAS 265, 664 /bibitem Greiner J., Schwarz R., Zharikov S., Orio M., 2000, A&A in press (astro-ph/0009430)
 Grupe D., Beuermann K., Mannheim K., et al., 1995a, A&A 299, L5
 Grupe D., Beuermann K., Mannheim K., et al., 1995b, A&A 300, L21
 Grupe D., Beuermann K., Mannheim K., Thomas H.-C., Fink, H.H., 1998a, A&A 330, 25
 Grupe D., Wills B.J., Wills D., Beuermann, K., 1998b, A&A 333, 827
 Grupe D., Beuermann K., Mannheim K., Thomas H.-C., 1999a, A&A 350, 805
 Grupe D., Thomas H.-C., Leighly K.M., 1999b, A&A 350, L31
 Grupe D., Wills B.J., Wills D., 1999c, ASP Conference Series Vol. 175, p347
 Grupe D., Leighly K.M., Thomas H.-C., Laurent-Muehleisen S.A., 2000a, A&A 356, 11
 Grupe D., Thomas H.-C., Leighly K.M., 2000b, A&A submitted
 Komossa S., Bade N., 1999, A&A 343, 775
 Komossa S., Greiner J., 1999, A&A 349, L45
 Komossa S., Meerschweinchen J., 2000, A&A 354, 411
 Lawrence A., Pye J.P., Elvis M., 1977, MNRAS 181, 93P
 Lawrence A., Papadakis I., 1993, ApJ 414, L85
 Leighly K.M., Mushotzky R.F., Yaqoob T., Kunieda H., Edelson R., 1996, ApJ 469, 147
 Leighly K.M., 1999a, ApJS 125, 297
 Leighly K.M., 1999b, ApJS 125, 317
 Nandra K., George I.M., Mushotzky R.F., Turner T.J., Yaqoob T., 1997, ApJ 476, 70
 Peterson B.M., McHardy I.M., Wilkes B.J., et al., 2000 ApJ in press
 Pfeffermann E., Briel U.G., Hippmann H., et al., 1986, SPIE 733, 519
 Piro L., Massaro E., Perola G.C., Molteni D., 1988, ApJ 325, L25
 Pounds K. A., Allan D. J., Barber C., et al., 1993, MNRAS 260, 77
 Puchnarewicz E.M., Mason K.O., Córdova F.A., et al, 1992, MNRAS 256, 589
 Rees M.J., 1990, Science 247, 817.
 Ross R.R., Fabian A.C., Mineshige S., 1992, MNRAS 258, 189
 Thomas H.-C., Beuermann K., Reinsch K., et al., 1998, A&A 335, 467
 Trümper J., 1983, Adv. Space Res. 4, 241
 Voges W., Aschenbach B., Boller Th., et al., 1999, A&A 349, 389
 Zimmermann U., Boese G., Becker W., et al., 1998, EXSAS User’s Guide, MPE Report (<http://wave.xray.mpe.mpg.de/exsas/users-guide>)